Activation Mode and Origin of Selectivity in Chiral Phosphoric Acid-Catalyzed Oxacycle Formation by Intramolecular Oxetane Desymmetrizations

Rajat Maji,[†]Pier Alexandre Champagne,[‡] K. N. Houk[‡*] and Steven E. Wheeler[†§*]

[†]Department of Chemistry, Texas A&M University, College Station, TX, 77842

[‡]Department of Chemistry and Biochemistry, University of California, Los Angeles, CA 90095

[§]Center for Computational Quantum Chemistry, Department of Chemistry, University of Georgia, Athens, GA 30602

Supporting Information Placeholder

ABSTRACT: Density functional theory methods were used to elucidate the activation mode and origin of stereoselectivity in chiral phosphoric acid-catalyzed intramolecular oxetane desymmetrizations. Computed enantioselectivities are in excellent agreement with experiment. An unexpected, distortion-driven activation mode was observed, instead of the usual "bifunctional activation." This mode is only favored for some intramolecular oxetane openings, highlighting an exception to known models. Stereoselectivity in these reactions can be explained by the balance of favorable non-covalent interactions of the substrates with both the aryl substituents and phosphoric acid functionality of the catalysts.

INTRODUCTION

The desymmetrization of achiral and *meso* compounds is a powerful route to enantiopure molecules, and has consequently received significant attention.[1] While intermolecular oxetane openings provide access to 2,3-disubstituted propan-1-ols,[2] intramolecular variants of this reaction can incorporate these scaffolds into cyclic structures. Numerous strategies for enantioselective oxetane openings have been developed, involving organocatalysts,[3] Lewis acids,[4] and metals.[5] A more complete understanding of key stereocontrolling factors in such reactions, as well as deeper mechanistic insights, will help to expand the scope of these synthetic protocols.

Computational quantum chemistry has emerged as a powerful means of achieving such insights across many classes of organocatalyzed reactions,[6] including those catalyzed by chiral phosphoric acids (CPAs).[7] The last decade has witnessed significant progress in our understanding of CPA-catalyzed reactions,[8] particularly in terms of their preferred activation mode and origins of stereoselectivity.[9] Complemented by experimental work by Gschwind *et al.*,[10] theoretical studies have provided key insights into the binding modes of these catalysts and the development of intuitive models that enable the prediction and rationalization of stereochemical outcomes for many of these reactions.[8b,11] The general consensus is that CPA-catalyzed reactions typically operate via a 'bifunctional' activation mode[8f,12] in which the electrophile and nucleophile are simultaneously activated through interactions with the Brønsted acidic and basic sites of the catalyst.[9] Concurrently, the understanding of the origin of stereoselectivity of these reactions has gradually shifted from a view anchored in repulsive steric interaction to more nuanced models based on the interplay of numerous attractive and repulsive non-covalent interactions between the catalyst and substrates.[13]

Recently, Seguin and Wheeler[14] and Champagne and Houk[15] presented theoretical studies of CPA-catalyzed intermolecular oxetane ring openings, reaching disparate conclusions regarding the relative importance of distortion effects and non-covalent interactions. In particular, Seguin and Wheeler[14] found that electrostatic interactions guided the selectivity of oxetane ring openings in the case of mercaptobenzothiazole nucleophiles,[16] while Champagne and Houk[15] reported a distortion-guided steric outcome for HCl mediated oxetane ring openings.[17] The latter study provided a general model of selectivity for oxetane desymmetrizations, which correctly explains the major enantiomer observed in various published reactions of oxetanes, including the one studied by Seguin and Wheeler.[14]

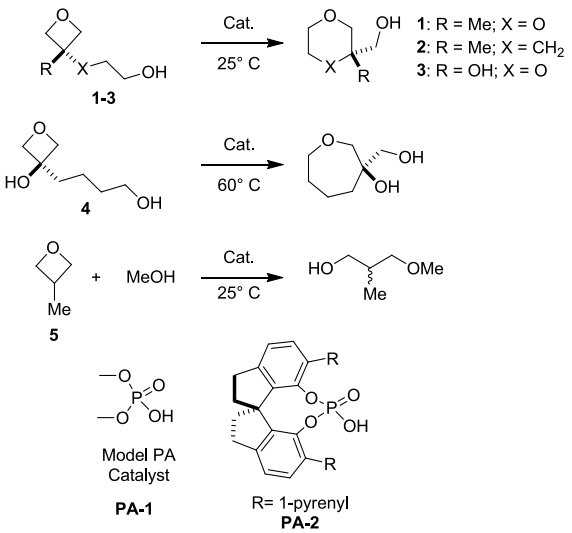

Scheme 1. Intramolecular oxetane ring opening reactions from Sun *et al.*[18] (substrates 1-4), along with a model intermolecular oxetane ring opening (substrate 5).

However, this general model of selectivity was not directly applicable to Sun's intramolecular openings of 3,3-disubstituted oxetanes (Scheme 1).[18] Intrigued by this limitation of the model, and in line with our overlapping interests in CPA-catalyzed reactions,[13f,13i,13k,19]

we pursued a joint theoretical study of the intramolecular oxetane desymmetrizations in Scheme 1.[18] These reactions provide direct access to enantioenriched 1,4-dioxanes and other related oxacycles that are abundant in natural products and pharmaceuticals. For these reactions, (*R*)-SPINOL-derived catalyst **PA-2** was the most selective, and good yields of the desired products were usually obtained at room temperature. To explain the experimental selectivity, Sun *et al.*[18] assumed the conventional bifunctional activation mode, where the stereochemical outcome could be predicted through consideration of steric interactions. However, since our recently-developed steric model could not account for the observed selectivity[15] we expected to find some caveat to this explanation.

THEORETICAL METHODS

All DFT computations were carried out using Gaussian 09.[20] Geometry optimizations and vibrational frequency computations were conducted at the B97D/TZV(2d,2p) level of theory, with single point energy refinements at the M06-2X/6-311+G(d,p) level. Solvent effects (dichloroethane) were accounted for with SMD for all geometry optimizations, vibrational frequency computations, and single-point energies unless specified otherwise.[21] Stereoselectivities were based on the relative free energies of the lowest-lying transition state (TS) structures leading to the minor and major stereoisomers ($\Delta\Delta G^{\ddagger}$), under the assumption that these reactions are under Curtin-Hammett control. Transition state structures were verified by the presence of a single imaginary vibrational frequency. The theoretical free energy differences for each reaction/catalyst combination are based on an extensive search of possible conformations of the catalyst and substrates (see SI for more details). Thermal free energy corrections were based on the quasi-rigid rotor/harmonic oscillator (quasi-RRHO) approximation of Grimme.[22] The overall energetic profile of the catalytic cycle was analyzed by applying the energetic span model.[23] Distortion/interaction analysis was performed on the B97-D/TZV(2*d*,2*p*) optimized geometries following the protocol of Ess and Houk[24] (or equivalently, the activation-strain model of Bickelhaupt *et al.*[25]). AIM analyses have been employed to identify important non-covalent interactions,[26] and the strength of various hydrogen bonding interactions were quantified using the method by Espinosa and coworkers.[27] NCI plots were also used to visualize dispersion-driven non-covalent interactions as proposed by Yang and coworkers.[28] Atomic charges were computed using natural population analysis (NPA).[29] The electrostatic stabilization was quantified by taking the product of the electrostatic potential (ESP) due to all other atoms evaluated at the position of a proton with the NPA atomic charge of the proton in the intact TS structure, as done previously by Lu and Wheeler.[30] Molecular structure figures were generated using CYLview.[31]

RESULTS AND DISCUSSION

To evaluate the possible activation modes in CPA-catalyzed intramolecular oxetane desymmetrizations, we first considered the reaction of substrate **1** catalyzed by phosphoric acid dimethyl ester (**PA-1**) as a model catalyst.[32] Three low-energy binding modes were identified, and the most stable conformations for each mode are shown in **Figure 1** in a rotated Goodman[11a] and Terada-Himo quadrant[8b,33] projections. These projections are related by a 90° rotation along the x-axis. A nearly linear arrangement of the leaving group, substituted carbon, and nucleophile is observed in all three cases, as expected for an S_N2-like opening of the oxetane. In these transition states, proton transfer to the oxetane oxygen is complete, while the nucleophilic alcohol is still almost intact (both O–H bonds are between 0.97 – 1.03 Å), an effect related to the weak acidity of alcohols. The result is that these TSs are essentially ion-pairs of the protonated substrate and deprotonated catalyst.[10b,10c,34] Notably, the chair-like conformation of the forming 6-membered ring is always the most favorable. After the TS, IRC analysis shows that the cationic product is deprotonated by the catalyst phosphate to form a neutral product-complex spontaneously.

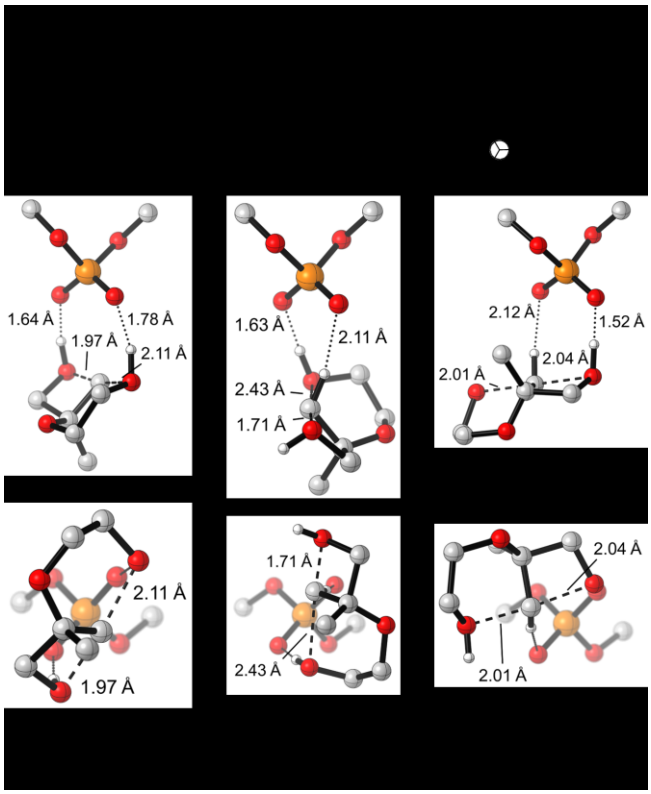

Figure 1. Three activation modes of substrate **1** catalyzed by **PA-1**, shown in their rotated Goodman (middle row) and quadrant (bottom row) projections, with their (relative) free energies of activation (in kcal/mol). Non-critical hydrogens are omitted for clarity (note that in the Goodman projection for the OA mode, a proton is obscured by the nucleophilic oxygen). The TSs shown lead to the (*S*)-product.

In addition to the expected "bifunctional activation" (**BA**) mode,[13k,14-15] we found two unprecedented modes where the catalyst interacts with only one of the two OH groups. In the "nucleophile activation" (**NA**) mode, only the nucleophile OH is bound to the phosphate, while in the "oxetane activation" (**OA**) mode, the oxetane OH is bound to the phosphate. In both cases however, the second oxygen of the catalyst engages in a CH···O interaction with the carbon undergoing substitution. Surprisingly, in this intramolecular system, **OA** is the most favorable activation mode, with an activation free energy of 32.7 kcal/mol compared to separated reactants. This is 0.9 and 1.1 kcal/mol smaller than the activation free energy for the **BA** and **NA** modes, respectively. Although the **OA** mode is preferred for this reaction, due to the lack of a substantial energy difference we were unable to eliminate the other possible activation modes at this stage.

The **BA** mode has two strong OH···O hydrogen bonds between the catalyst oxygens and the substrate, yet has similar energies to **NA** or **OA**. To understand this effect, we conducted a distortion/interaction analysis at the SMD-M06-2X/6-311+G(d,p) level of theory (Table 1). We compared the relative energies of distortion of the catalyst ($\Delta\Delta E^{t}_{st}$) and substrate ($\Delta\Delta E^{b}_{st}$) components, as well as the actual

(ΔE_{int}) and relative ($\Delta\Delta E_{int}$) interaction energies between these two parts, setting the **BA** mode as our standard (0.0 kcal/mol).

Table 1. Relative distortion/interaction analysis (in kcal/mol).

TS	$\Delta\Delta E^{\ddagger}$	$\Delta\Delta E^{t}_{st}$	$\Delta\Delta E^{b}_{st}$	ΔE_{int}	$\Delta\Delta E_{int}$
BA	0.0	0.0	0.0	-38.0	0.0
NA	0.4	-0.3	-14.4	-22.9	15.1
OA	-0.6	0.0	-9.9	-28.7	9.3

No difference in the catalyst distortion was identified by this analysis, but drastically different substrate distortion energies were found. Interestingly, the **BA** mode requires the most substrate distortion, whereas the **NA** and **OA** modes require 14.4 and 9.9 kcal/mol less substrate distortion, respectively. However, this reduced distortion for **NA** and **OA** comes at the cost of reduced interaction energies with the catalyst, as expected from the different binding patterns exhibited by these activation modes (Figure 1). For **OA**, the reduction in interaction energy is only slightly smaller (9.3) than the savings from distortion (-9.9), making it the best activation mode by a mere 0.6 kcal/mol.

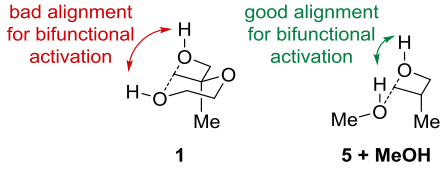

Figure 2. Different alignments of the OH groups for intra- and intermolecular oxetane desymmetrizations.

The distortion required for the intramolecular ring system of **1** can be explained by the nature of the forming 6-membered ring, which involves all sp^3-hybridized atoms. This precludes the alignment of the oxetane and nucleophile O–H bonds required to simultaneously engage in strong hydrogen bonding interactions with the phosphate catalyst in the **BA** mode (**Figure 2**). Instead, significant distortions of the oxetane and chair-like rings are required for these hydrogen bonds to align. To prove this, we computed TS structures for the reaction of substrate **5** with methanol, again catalyzed by model catalyst **PA-1** (**Figure 3**). In this case, easy alignment of both OH groups was expected (**Figure 2**).

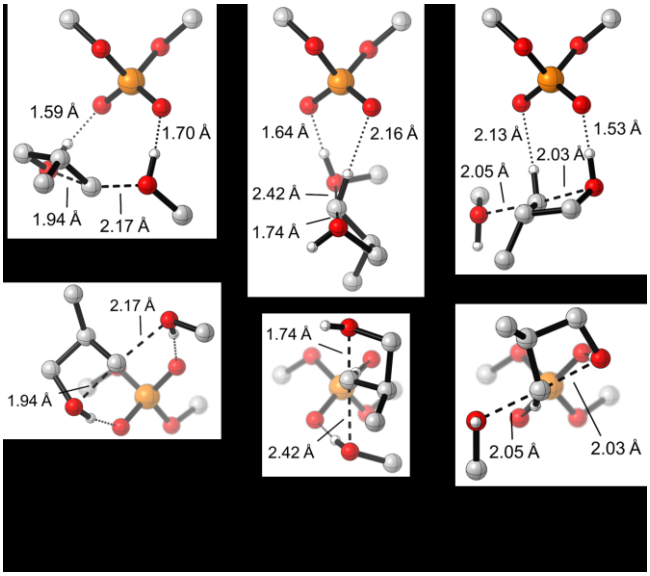

Figure 3. Rotated Goodman and quadrant projections of the three activation modes, for the reaction of **5** with MeOH, catalyzed by **PA-1**. Non-critical hydrogens are removed for clarity. (Relative) free energies of activation are displayed below the structures, in kcal/mol.

Indeed, for this model system, the **BA** mode is at least 3.2 kcal/mol more favorable than either **NA** or **OA**. When these intermolecular TS structures are compared to those of **Figure 1**, the **NA** and **OA** modes have identical alignments of the nucleophilic and electrophilic parts of the reaction, relative to the catalyst structure. Therefore, for these modes, the intra- or intermolecular nature of the TS has no effect. However, the **BA** TS is organized in a strikingly different way in Figures 1 and 3, which indicates that it is arranged differently, depending on whether the reaction is intramolecular (distorted) or intermolecular (not distorted). Therefore, *in the absence of unfavorable distortion, the conventional bifunctional mode is the preferred mode of activation for the opening of oxetanes catalyzed by phosphoric acids.*

Having established the plausibility of several potential binding modes for intramolecular oxetane ring openings, we next considered four examples using the full catalyst **PA-2**. Theoretical *ee*'s are presented in Table 2; we are pleased to observe remarkable agreement with the experimental stereoselectivities,[18] capturing not only the reduced stereoselectivity for substrates 3 and 4 but also reasonable reproduction of experimental values in all cases. Computed *ee* values are 1-16% lower than experimental, representing a maximum error of 0.6 kcal/mol.

Table **2**. Experimental[18] and theoretical *ee*'s and corresponding relative free energies (in kcal/mol) for substrates **1**-**4** catalyzed by **PA-2**.[a]

	Experiment		Theory	
Substrate	*ee*	$\Delta\Delta G^{\ddagger}$	*ee*	$\Delta\Delta G^{\ddagger}$
1	98	2.7	94	2.1
2	91	1.8	90	1.8
3	86	1.5	78	1.3
4	67	1.1	51	0.7

[a]All reactions at 298K except for substrate **4** (333K).

For the reaction of substrate **1** catalyzed by the real catalyst **PA-2**, the same three activation modes can be located, but their relative energies are significantly different from those computed for **PA-1** (**Figure 4**). Notably, **OA** is even more strongly favored over the other activation modes for the real catalyst than for the model catalyst, indicating that the flanking pyrenyl groups provide greater stabilization to the TS for the **OA** mode. We find that in both **NA** and **OA**, the OH group that is not bound to the PA moiety is engaged in an OH···π interaction with one of the flanking pyrenyl groups of the catalyst, partially offsetting the decreased interaction energy inherent to these two activation modes (see above). Of interest, the arrangement of the substrate relative to the catalyst structure is almost identical, *whether the real or model catalyst is used*, except for slight variations that allow a more efficient OH···π overlap.

Additional insights regarding this preferred binding mode can be gleaned from distortion/interaction analysis. As in the model TS structures, interaction energies favor the **BA** mode, in large part because of the presence of two OH···O hydrogen bonds; however, this comes at the expense of distortion of the substrate in order to align these two hydrogen bonds with the phosphate oxygens. In the **OA** mode, the less favorable hydrogen bonding interactions are compensated by the lack of distortion. Moreover, in this mode there is an additional stabilization afforded by the OH···π interaction between

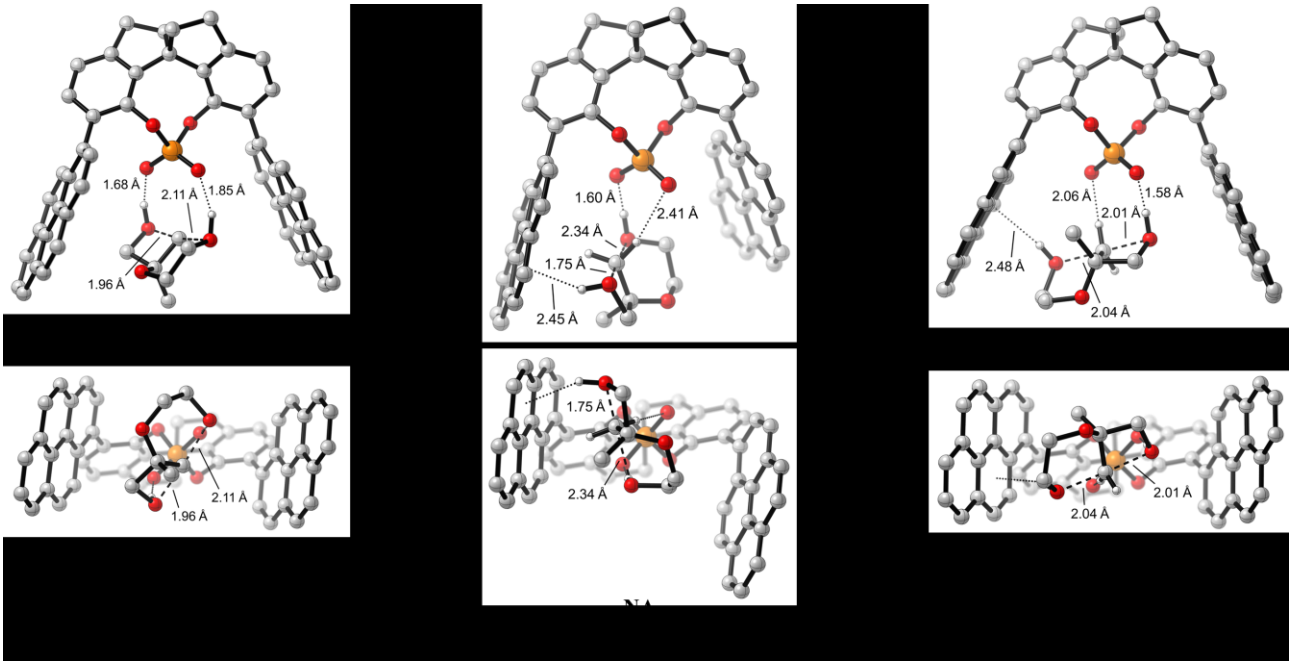

Figure 4. Lowest-energy TSs for reaction of substrate **1** catalyzed by **PA-2** for the three activation modes, shown in their rotated Goodman (top row) and quadrant (bottom row) projections. The structures shown lead to the major (*S*) product found experimentally. (Relative) free energies of activation are given below the structures, in kcal/mol. Key bond lengths are highlighted. Non-critical hydrogen atoms are omitted for clarity.

the nucleophilic OH and one of the pyrenyl substituents on the catalyst. The net result is that for reactions catalyzed by **PA-2**, the TS structures corresponding to the **BA** mode are thermodynamically unimportant and these reactions proceed almost entirely via **OA**. We note that these trends are consistent regardless of the DFT method employed (see SI Table S2).

Considering the overall free energy profile for reaction of **1**, the energetic span[23] for the catalyzed reaction is 23.9 kcal/mol and the reaction is exergonic by 20.7 kcal/mol (see SI Figure S1). This relatively low energetic span can be contrasted with the uncatalyzed reaction (47.3 kcal/mol), or the span resulting from the model catalyst **PA-1** (32.7 kcal/mol). In other words, the non-covalent stabilization of the rate-limiting TS provided by the aryl substituents on the catalyst is a vital component of the catalytic activation of this reaction; the phosphoric acid functionality alone does not lower the barrier enough to render this intramolecular oxetane ring opening viable at room temperature.

Finally, we turn to understanding the mode of stereoinduction for the reaction of substrates **1**-**4** catalyzed by **PA-2**. The lowest-lying TS structures leading to the major (*S*) and minor (*R*) stereoisomers are shown in Figures 5 and 6 for substrates **1** and **3**, respectively (see SI Figure S2 for TS structures for **2** and **4**). First, these favored TS structures correspond to the **OA** mode, in which the oxetane interacts with the catalyst via OH···O and C–H···O interactions with the phosphate. It is instructive to compare the substrate orientations in these TS structures for **PA-2** with the corresponding structures for the model catalyst **PA-1** (see Figure 5). For **1**, in the TS leading to the major (*S*) product, the reacting substrate adopts an arrangement that is almost identical to that seen for the model catalyst (Figure 5a). A slight shift of the substrate and rotation of the nucleophilic OH orient this hydroxyl group towards the nearby pyrene, leading to a more stabilizing OH···π interaction. However, in the TS leading to the minor (*R*) product the substrate is oriented differently in the model and real catalysts (Figure 5b). To achieve a moderately good OH···π overlap, the substrate is rotated within the pocket, which has the effect of elongating and thus weakening the CH···O interaction that is characteristic of the **OA** mode [2.42 Å in TS(*R*) vs 2.06 Å in TS(*S*)]. Furthermore, if the substrate were to adopt the orientation seen with the model catalyst in the pocket of **PA-2**, the methyl substituent would be in close contact with the wall of the catalyst. This further incentivizes the above-mentioned rotation.

Overall, due to the two-point binding of the TSs in **OA**, which imposes a predictable arrangement of the substrate, the TS leading to the major stereoisomer positions the nucleophilic OH group in an arrangement favorable for OH···π interaction, while the TS leading to the minor enantiomer has to rotate to engage in such an interaction. Based on the importance of these stabilizing OH···π interactions in these TS structures (see above), a model can be developed to qualitatively explain the sense of the observed enantioselectivity. This model is shown in **Figure 7a**.

As the **OA** mode uses a relatively weak CH···O interaction to bind the substrate to the catalyst, any possibly stronger interaction has the potential to displace this CH···O interaction and alter the substrate orientation. For instance, substrates **3** and **4** feature an OH group at the 3-position, which is capable of hydrogen bonding with the catalyst. Figure 6 shows that in the lowest-energy TS structures of **3** with **PA-2**, the substrate is oriented to allow the protonated oxetane and 3-OH groups to interact with the phosphate moiety. However, as this new binding mode is governed by these two non-covalent interactions, the expected arrangements of the TSs are predictable. This allows us to draw another model to explain the observed selectivity for these substrates (**Figure 7b**). This model is once again based on the fact that the OH···π interaction is crucial to stabilize the TSs, such that the minor TSs will have to rearrange in the catalyst pocket to maximize this interaction.

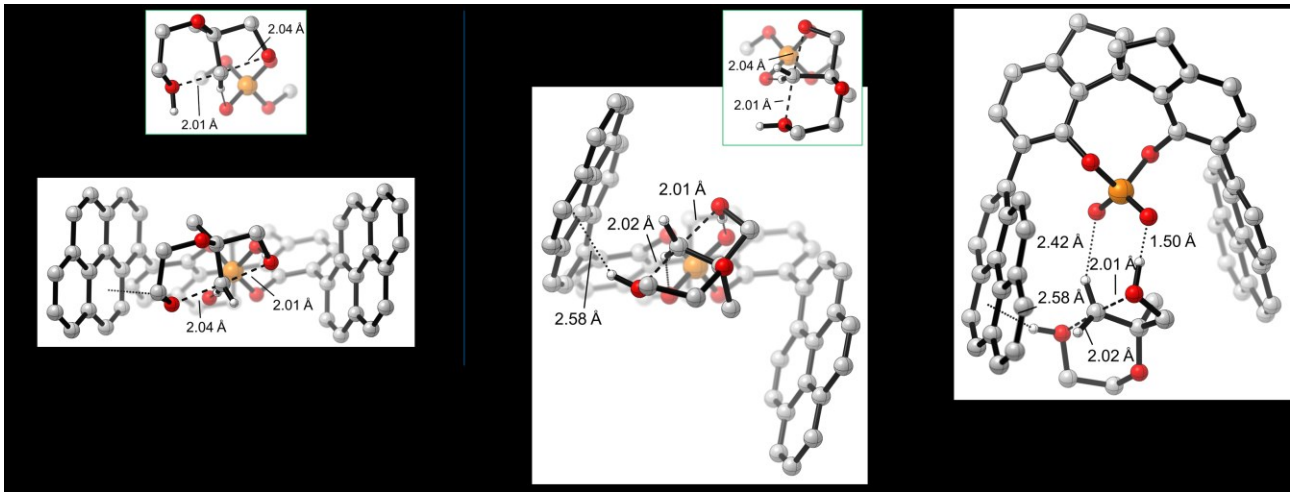

Figure 5. Lowest-lying stereocontrolling TS structures for the reaction of **1** catalyzed by **PA-2**. a) Quadrant projection of the TS structures leading to the major (*S*)-product. Inset: Lowest-energy (*S*) TS structure with model catalyst **PA-1**. b) Quadrant (left) and rotated Goodman (right) projections of the TS structures leading to the minor (*R*) product. Inset: Lowest-energy (*R*) TS structure with the model catalyst. Non-critical hydrogens are omitted for clarity.

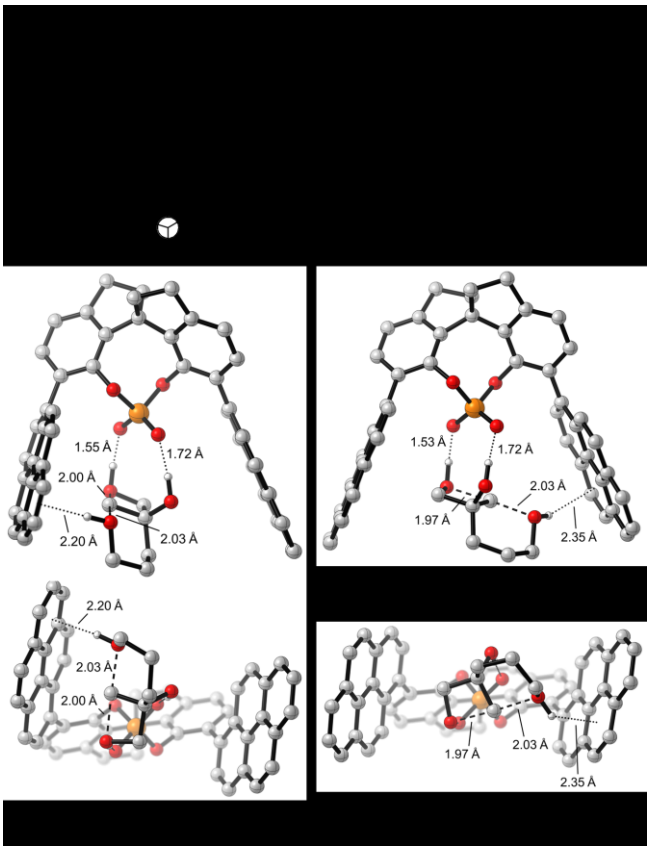

Figure 6. Most favorable TS structures leading to each enantiomer for the reaction of **3** catalyzed by **PA-2**. Structures are shown in their rotated Goodman (middle row) and quadrant (bottom row) projections, with non-critical hydrogens removed for clarity.

Distortion/interaction analyses[24-25] provide further quantitative insight into the mode of stereoinduction in these reactions, adding to the above discussion and the associated models in Figure 7. Gas-phase energy differences between the lowest-lying TS structures leading to the minor and major stereoisomers, $\Delta\Delta E^{\ddagger}$ (Table 3), follow a similar trend to the $\Delta\Delta G^{\ddagger}$ values from Table 2, indicating only a small impact of solvent and entropic effects on stereoselectivity. To understand the origin of these gas-phase energy differences, they were decomposed into the difference in energy required to distort the catalyst ($\Delta\Delta E_{st}^{\ddagger}$) and substrates ($\Delta\Delta E_{st}^{\ddagger}$) into the corresponding TS geometries, and the difference in interaction energies between these distorted species (see Table **3**). For substrates **1**-**3**, substrate distortion favors formation of the minor stereoisomer (for **4**, substrate distortion has no significant effect); however, these effects are overshadowed by the catalyst distortion, which favors the TS structures leading to the major stereoisomer. In all cases, the largest driver of stereoselectivity is differences in interaction energies between the substrates and catalyst, which favor the TS structures leading to the major stereoisomer.

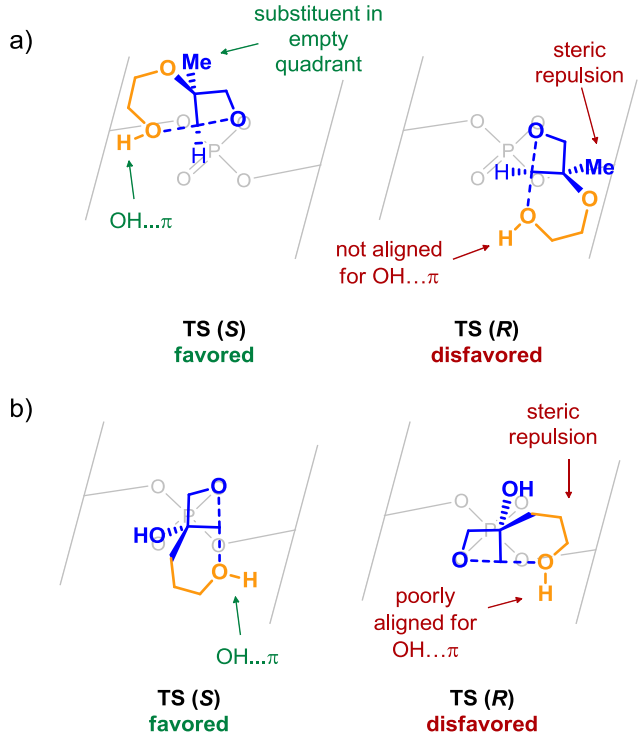

Figure 7. Models depicting the expected arrangements of substrates **1** (a) and **3** (b) relative to the binding pocket of a CPA catalyst. Comparison of these structures allow a qualitative understanding of which enantiomer will be favored.

These interaction energy contributions to $\Delta\Delta E^{\ddagger}$ were further probed by considering truncated model systems in which the substrate interacts with either the pyrenyl groups ($\Delta\Delta E^{\ddagger}_{t}$) or phosphoric acid functionality ($\Delta\Delta E^{\ddagger}_{t}$), in the geometries of the stereocontrolling TS structures (see Table 3). These models provide a rough separation of the contribution of non-covalent interactions with the aryl substituents and phosphoric acid functionality to $\Delta\Delta E_{int}$, respectively. For substrate **1**, non-covalent interactions between the substrate and pyrenyl groups have no net impact on stereoselectivity; instead, the energy difference between the stereocontrolling TS structures arises from differences in non-covalent interactions with the phosphoric acid component of the catalyst. This is consistent with the model in Figure 7a. For substrate **1**, both stereocontrolling TSs feature similar OH···π interactions with the aryl walls of the catalyst, but in the minor TS the CH···O interaction is elongated to afford the proper geometry. This is reflected in $\Delta\Delta E^{\ddagger}_{t}$. Substrates **2**-**4** are more complicated, since non-covalent interactions with the aryl substituents and phosphoric acid functionality both impact the stereoselectivity. While interactions with the aryl groups favor the major TS for all three of these substrates, interactions with the phosphate favor the major TS for **2** but the minor TS for substrates **3** and **4**. Analyses by AIM[26b,33] and NCI[28] support the finding that non-covalent interactions of the substrate with the aryl walls of the catalyst preferentially stabilize the major TS and enhance the stereoselectivity. In particular, while non-covalent interactions abound in both the major and minor TS, AIM and NCI indicated that the major TS features stronger CH···π, OH···π, and (in the case of substrates **3** and **4**) lone pair···π interactions than the minor TS.

Table 3. Differences in gas-phase energies ($\Delta\Delta E^{\ddagger}$) between the stereocontrolling TS structures, decomposition of $\Delta\Delta E^{\ddagger}$ into distortion ($\Delta\Delta E^{t}_{st}$ and $\Delta\Delta E^{b}_{st}$) and interaction ($\Delta\Delta E_{int}$) energies, and approximate decomposition of $\Delta\Delta E_{int}$ into contributions from non-covalent interactions of the substrates with the aryl ($\Delta\Delta E^{\ddagger}_{t}$) and phosphoric acid ($\Delta\Delta E^{\ddagger}_{t}$) components of the catalyst.

Sub.	$\Delta\Delta E^{\ddagger}$	$\Delta\Delta E^{t}_{st}$	$\Delta\Delta E^{b}_{st}$	$\Delta\Delta E_{int}$	$\Delta\Delta E^{\ddagger}_{t}$	$\Delta\Delta E^{\ddagger}_{t}$
1	4.8	2.9	-1.0	2.9	-0.1	4.1
2	5.5	2.1	-0.9	4.4	3.2	1.2
3	1.1	0.5	-0.5	1.1	2.9	-1.3
4	1.6	0.6	0.2	0.8	2.6	-2.5

Differences in the interactions of the substrate with the phosphoric acid functionality, which favor formation of the major stereoisomer for **1** and **2** but the minor stereoisomer for **3** and **4**, can be understood by considering the partial atomic charges and geometries of the corresponding TS structures. In the **OA** mode, the early protonation of the substrate by the catalyst leads to substantial partial positive charges on the hydrogens of the carbon being attacked; these charges will interact with the chiral electrostatic environment created by the deprotonated catalyst, as observed recently by Seguin and Wheeler[13k] and List *et al.*[35] for CPA catalyzed epoxide desymmetrizations. These electrostatic contributions are associated with the CH···O interactions between the substrate and catalysts in the major and minor TS structures. For substrates **1** and **2**, there is a greater positive charge and a shorter CH···O distance in the TS leading to the major stereoisomer, compared to the minor product (see Figure 8). This trend is reversed for substrates **3** and **4**, for which the TS leading to the minor stereoisomer exhibits a geometry more compatible with electrostatic stabilization via this CH···O interaction.

These electrostatic effects can be quantified approximately by considering the interaction of these atomic charges with the electrostatic potential arising from the deprotonated catalyst (see Figure 8). The resulting difference in electrostatic interactions for substrate **1**, accounting for the CH···O and OH···O interactions, is +2.8 kcal/mol (favoring the major stereoisomer); for substrate **3** (accounting for both OH···O interactions and the CH···O), the difference in electrostatic stabilization is -1.9 kcal/mol (favoring the minor stereoisomer). This can be contrasted with the aforementioned work[13k,35] on CPA-catalyzed epoxide ring openings, where the stereoselectivity was uniformly enhanced by the electrostatic stabilization of the TS structure leading to the major stereoisomer.

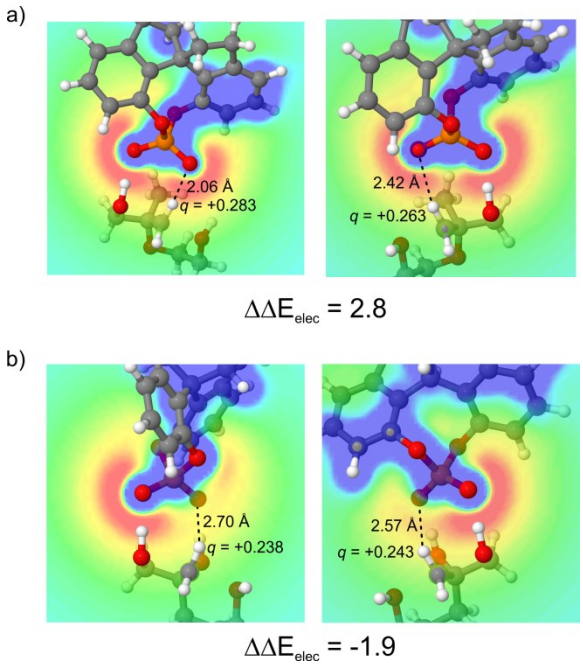

Figure 8. Electrostatic potentials due to the deprotonated catalyst in the plane of key hydrogens (red = -150.0 kcal/mol; blue = 0.0 kcal/mol). The difference in electrostatic stabilization for substrate **1** (a) and **3** (b) of the key CH and OH group(s) ($\Delta\Delta E_{elec}$) is also shown in kcal/mol.

CONCLUSIONS

We have shown that the activation mode for chiral phosphoric acid-catalyzed intramolecular oxetane ring openings differs qualitatively from that for intermolecular oxetane ring openings, and is contrary to popular reactivity models for CPA-catalyzed reactions in general. The origin of this is straightforward: intramolecular oxetane desymmetrizations with all-sp^3 rings require significant substrate distortion in order for both the electrophile and nucleophile to engage in OH···O hydrogen bonds with the Brønsted acidic and basic sites of the catalyst. Instead, the favored activation mode for a series of intramolecular oxetane ring openings involves activation of only the oxetane by the phosphoric acid functionality; the nucleophile is mildly activated by OH···π interactions with a flanking pyrenyl group of the catalyst. This is corroborated by studies of a model intermolecular oxetane ring opening, for which the conventional bifunctional activation mode is favored.

From a mechanistic point of view, the intramolecular oxetane desymmetrization involves general acid catalysis. We have developed two models that qualitatively explain and predict which enantiomer will be favored for each type of substrate. Stereoselectivity of these reactions is driven primarily by differences in non-covalent interactions of the substrates with both the aryl substituents and phosphoric acid functionality of the catalysts. We showed that depending on the nature of groups attached, electrostatic interactions of the reacting oxetane with the chiral electrostatic environment of the deprotonated catalyst can either enhance or decrease the stereoselectivity. These intramolecular oxetane openings add to the growing list of organocatalysts that achieve selectivity through stabilizing non-covalent[36] and electrostatic interactions.[13k,37] We envision that the insights into the mode of stereoinduction in these reactions will prove useful in improving the scope and efficiency of related reactions.

ASSOCIATED CONTENT

Supporting Information

The Supporting Information is available free of charge on the ACS Publications website. Additional computational details and data, absolute free energies, additional figures, and optimized Cartesian coordinates.

AUTHOR INFORMATION

Corresponding Authors

*houk@chem.ucla.edu
*swheele2@uga.edu

ACKNOWLEDGMENT

This work was supported by National Science Foundation (Grants CHE-1266022 and CHE-1665407 to S.E.W and CHE-1361104 to K.N.H.). P.A.C gratefully acknowledges the Fonds de recherche du Québec, Nature et Technologies (FRQNT) for a postdoctoral fellowship. We thank T. J. Seguin for fruitful discussions. Portions of this research were conducted with resources from the Texas A&M Supercomputing Center, the Hoffman2 cluster at UCLA, and the Extreme Science and Engineering Discovery Environment (XSEDE), which is supported by the NSF (OCI-1053575).

REFERENCES

(1)(a) Zeng, X.-P.; Cao, Z.-Y.; Wang, Y.-H.; Zhou, F.; Zhou, J. *Chem. Rev.* **2016**, *116*, 7330-7396; (b) Diaz de Villegas, M. D.; Galvez, J. A.; Etayo, P.; Badorrey, R.; Lopez-Ram-de-Viu, P. *Chem. Soc. Rev.* **2011**, *40*, 5564-5587.
(2)Bull, J. A.; Croft, R. A.; Davis, O. A.; Doran, R.; Morgan, K. F. *Chem. Rev.* **2016**, *116*, 12150-12233.
(3)(a) Yin, Q.; You, S.-L. *Org. Lett.* **2014**, *16*, 1810-1813; (b) Chen, Z.; Wang, Z.; Sun, J. *Chemistry – A European Journal* **2013**, *19*, 8426-8430; (c) Chen, Z.; Wang, B.; Wang, Z.; Zhu, G.; Sun, J. *Angew. Chem. Int. Ed.* **2013**, *52*, 2027-2031.
(4)Yadav, J. S.; Singh, V. K.; Srihari, P. *Org. Lett.* **2014**, *16*, 836-839.
(5)(a) Gronnier, C.; Kramer, S.; Odabachian, Y.; Gagosz, F. *J. Am. Chem. Soc.* **2012**, *134*, 828-831; (b) Ruider, S. A.; Müller, S.; Carreira, E. M. *Angew. Chem. Int. Ed.* **2013**, *52*, 11908-11911; (c) Mizuno, M.; Kanai, M.; Iida, A.; Tomioka, K. *Tetrahedron* **1997**, *53*, 10699-10708.
(6)Jang, K. P.; Hutson, G. E.; Johnston, R. C.; McCusker, E. O.; Cheong, P. H. Y.; Scheidt, K. A. *J. Am. Chem. Soc.* **2014**, *136*, 76-79.
(7)Straker, R. N.; Peng, Q.; Mekareeya, A.; Paton, R. S.; Anderson, E. A. *Nat Commun* **2016**, *7*.
(8)(a) Yamanaka, M.; Itoh, J.; Fuchibe, K.; Akiyama, T. *J. Am. Chem. Soc.* **2007**, *129*, 6756-6764; (b) Marcelli, T.; Hammar, P.; Himo, F. *Chemistry – A European Journal* **2008**, *14*, 8562-8571; (c) Simón, L.; Goodman, J. M. *J. Am. Chem. Soc.* **2008**, *130*, 8741-8747; (d) Yamanaka, M.; Hirata, T. *J. Org. Chem.* **2009**, *74*, 3266-3271; (e) Simón, L.; Goodman, J. M. *J. Am. Chem. Soc.* **2009**, *131*, 4070-4077; (f) Jindal, G.; Sunoj, R. B. *Angew. Chem. Int. Ed.* **2014**, *53*, 4432-4436; (g) Overvoorde, L. M.; Grayson, M. N.; Luo, Y.; Goodman, J. M. *The Journal of Organic Chemistry* **2015**, *80*, 2634-2640.
(9)Parmar, D.; Sugiono, E.; Raja, S.; Rueping, M. *Chem. Rev.* **2014**, *114*, 9047-9153.
(10)(a) Greindl, J.; Hioe, J.; Sorgenfrei, N.; Morana, F.; Gschwind, R. M. *J. Am. Chem. Soc.* **2016**; (b) Sorgenfrei, N.; Hioe, J.; Greindl, J.; Rothermel, K.; Morana, F.; Lokesh, N.; Gschwind, R. M. *J. Am. Chem. Soc.* **2016**, *138*, 16345-16354; (c) Fleischmann, M.; Drettwan, D.; Sugiono, E.; Rueping, M.; Gschwind, R. M. *Angew. Chem. Int. Ed.* **2011**, *50*, 6364-6369.
(11)(a) Reid, J. P.; Simón, L.; Goodman, J. M. *Acc. Chem. Res.* **2016**, *49*, 1029-1041; (b) Akiyama, T. *Chem. Rev.* **2007**, *107*, 5744-5758.
(12)(a) Changotra, A.; Sunoj, R. B. *Org. Lett.* **2016**, *18*, 3730-3733; (b) Simón, L.; Goodman, J. M. *The Journal of Organic Chemistry* **2011**, *76*, 1775-1788; (c) Reid, J. P.; Goodman, J. M. *J. Am. Chem. Soc.* **2016**.
(13)(a) Krenske, E. H.; Houk, K. N. *Acc. Chem. Res.* **2013**, *46*, 979-989; (b) Grayson, M. N.; Pellegrinet, S. C.; Goodman, J. M. *J. Am. Chem. Soc.* **2012**, *134*, 2716-2722; (c) Neel, A. J.; Hehn, J. P.; Tripet, P. F.; Toste, F. D. *J. Am. Chem. Soc.* **2013**, *135*, 14044-14047; (d) Grayson, M. N.; Goodman, J. M. *J. Am. Chem. Soc.* **2013**, *135*, 6142-6148; (e) Maity, P.; Pemberton, R. P.; Tantillo, D. J.; Tambar, U. K. *J. Am. Chem. Soc.* **2013**, *135*, 16380-16383; (f) Meng, S.-S.; Liang, Y.; Cao, K.-S.; Zou, L.; Lin, X.-B.; Yang, H.; Houk, K. N.; Zheng, W.-H. *J. Am. Chem. Soc.* **2014**, *136*, 12249-12252; (g) Jindal, G.; Sunoj, R. B. *Angew. Chem., Int. Ed. Engl.* **2014**, *53*, 4432-4436; (h) Kanomata, K.; Toda, Y.; Shibata, Y.; Yamanaka, M.; Tsuzuki, S.; Gridnev, I. D.; Terada, M. *Chem. Sci.* **2014**, *5*, 3515-3523; (i) Seguin, T. J.; Lu, T.; Wheeler, S. E. *Org. Lett.* **2015**, *17*, 3066-3069; (j) Ajitha, M. J.; Huang, K.-W. *Org. Biomol. Chem.* **2015**, *13*, 10981-10985; (k) Seguin, T. J.; Wheeler, S. E. *ACS Catal.* **2016**, *6*, 2681-2688; (l) Simon, L.; Paton, R. S. *Org. Biomol. Chem.* **2016**, *14*, 3031-3039.
(14)Seguin, T. J.; Wheeler, S. E. *ACS Catal.* **2016**, *6*, 7222-7228.
(15)Champagne, P. A.; Houk, K. N. *J. Am. Chem. Soc.* **2016**, *138*, 12356-12359.
(16)Wang, Z.; Chen, Z.; Sun, J. *Angew. Chem. Int. Ed.* **2013**, *52*, 6685-6688.
(17)Yang, W.; Wang, Z.; Sun, J. *Angew. Chem. Int. Ed.* **2016**, *55*, 6954-6958.
(18)Yang, W.; Sun, J. *Angew. Chem. Int. Ed.* **2016**, *55*, 1868-1871.
(19)(a) Rodríguez, E.; Grayson, M. N.; Asensio, A.; Barrio, P.; Houk, K. N.; Fustero, S. *ACS Catal.* **2016**, 2506-2514; (b) Wang, H.; Jain, P.; Antilla, J. C.; Houk, K. N. *The Journal of Organic Chemistry* **2013**, *78*, 1208-1215; (c) Nimmagadda, S. K.; Mallojjala, S. C.; Woztas, L.; Wheeler, S. E.; Antilla, J. C. *Angew. Chem. Int. Ed.* **2017**, *56*, 2454-2458.
(20)Washington, I.; Houk, K. N. *Angew. Chem. Int. Ed.* **2001**, *40*, 4485-4488.
(21)Marenich, A. V.; Cramer, C. J.; Truhlar, D. G. *The Journal of Physical Chemistry B* **2009**, *113*, 6378-6396.
(22)Grimme, S. *Chemistry- A European Journal* **2012**, *18*, 9955-9964.
(23)Kozuch, S.; Shaik, S. *Acc. Chem. Res.* **2011**, *44*, 101-110.
(24)(a) Ess, D. H.; Houk, K. N. *J. Am. Chem. Soc.* **2007**, *129*, 10646-10647; (b) Ess, D. H.; Houk, K. N. *J. Am. Chem. Soc.* **2008**, *130*, 10187-10198.
(25)(a) van Zeist, W.-J.; Bickelhaupt, F. M. *Org. Biomol. Chem.* **2010**, *8*, 3118-3127; (b) Bickelhaupt, F. M. *J. Comput. Chem.* **1999**, *20*, 114-128.
(26)(a) Bader, R. F. W. *Acc. Chem. Res.* **1985**, *18*, 9-15; (b) Bader, R. F. W. *Chem. Rev.* **1991**, *91*, 893-928; (c) Tognetti, V.; Joubert, L. *Phys. Chem. Chem. Phys.* **2014**, *16*, 14539-14550.
(27)Espinosa, E.; Molins, E.; Lecomte, C. *Chem. Phys. Lett.* **1998**, *285*, 170-173.
(28)(a) Johnson, E. R.; Keinan, S.; Mori-Sánchez, P.; Contreras-García, J.; Cohen, A. J.; Yang, W. *J. Am. Chem. Soc.* **2010**, *132*, 6498-6506; (b) Contreras-García, J.; Johnson, E. R.; Keinan, S.; Chaudret, R.; Piquemal, J.-P.; Beratan, D. N.; Yang, W. *J. Chem. Theory Comput.* **2011**, *7*, 625-632.
(29)Reed, A. E.; Curtiss, L. A.; Weinhold, F. *Chem. Rev.* **1988**, *88*, 899-926.
(30)Lu, T.; Wheeler, S. E. *Org. Lett.* **2014**, *16*, 3268-3271.
(31)Legault, C. Y. *CYLview, 1.0b*, Université de Sherbrooke, 2009.
(32)Diphenylphosphoric acid as a model catalyst resulted in similar results concerning the relative energies of these three activation modes. See SI.
(33)Gridnev, I.; Kouchi, M.; Sorimachi, K.; Terada, M. *Tetrahedron Lett.* **2007**, *48*, 497-500.
(34)(a) Kim, H.; Sugiono, E.; Nagata, Y.; Wagner, M.; Bonn, M.; Rueping, M.; Hunger, J. *ACS Catal.* **2015**, *5*, 6630-6633; (b) Merten, C.; Pollok, C. H.; Liao, S.; List, B. *Angew. Chem. Int. Ed.* **2015**, *54*, 8841-8845.

(35)Monaco, M. R.; Fazzi, D.; Tsuji, N.; Leutzsch, M.; Liao, S.; Thiel, W.; List, B. *J. Am. Chem. Soc.* **2016**, *138*, 14740-14749.
(36)(a) Wheeler, S. E.; Seguin, T. J.; Guan, Y.; Doney, A. C. *Acc. Chem. Res.* **2016**, *49*, 1061-1069; (b) Sunoj, R. B. *Acc. Chem. Res.* **2016**, *49*, 1019-1028; (c) Bhaskararao, B.; Sunoj, R. B. *J. Am. Chem. Soc.* **2015**, *137*, 15712-15722; (d) Reddi, Y.; Sunoj, R. B. *ACS Catal.* **2015**, *5*, 1596-1603; (e) Cook, T. C.; Andrus, M. B.; Ess, D. H. *Org. Lett.* **2012**, *14*, 5836-5839; (f) Johnston, C. P.; Kothari, A.; Sergeieva, T.; Okovytyy, S. I.; Jackson, K. E.; Paton, R. S.; Smith, M. D. *Nat Chem* **2015**, *7*, 171-177; (g) Paton, R. S. *Org. Biomol. Chem.* **2014**, *12*, 1717-1720; (h) Holland, M. C.; Paul, S.; Schweizer, W. B.; Bergander, K.; Mück-Lichtenfeld, C.; Lakhdar, S.; Mayr, H.; Gilmour, R. *Angew. Chem. Int. Ed.* **2013**, *52*, 7967-7971; (i) Knowles, R. R.; Jacobsen, E. N. *Proceedings of the National Academy of Sciences* **2010**, *107*, 20678-20685; (j) Uyeda, C.; Jacobsen, E. N. *J. Am. Chem. Soc.* **2011**, *133*, 5062-5075; (k) Kennedy, C. R.; Lin, S.; Jacobsen, E. N. *Angew. Chem. Int. Ed.* **2016**, n/a-n/a; (l) Armstrong, A.; Boto, R. A.; Dingwall, P.; Contreras-Garcia, J.; Harvey, M. J.; Mason, N. J.; Rzepa, H. S. *Chem. Sci.* **2014**, *5*, 2057-2071.
(37)(a) Lu, T.; Zhu, R.; An, Y.; Wheeler, S. E. *J. Am. Chem. Soc.* **2012**, *134*, 3095-3102; (b) Yang, H.; Wong, M. W. *J. Am. Chem. Soc.* **2013**, *135*, 5808-5818; (c) Nguyen, Q. N. N.; Lodewyk, M. W.; Bezer, S.; Gagné, M. R.; Waters, M. L.; Tantillo, D. J. *ACS Catal.* **2015**, *5*, 1617-1622; (d) Lee, K.; Silverio, D. L.; Torker, S.; Robbins, D. W.; Haeffner, F.; van der Mei, F. W.; Hoveyda, A. H. *Nat Chem* **2016**, *8*, 768-777; (e) Johnston, R. C.; Cheong, P. H.-Y. *Org. Biomol. Chem.* **2013**, *11*, 5057-5064; (f) Pattawong, O.; Mustard, T. J. L.; Johnston, R. C.; Cheong, P. H.-Y. *Angew. Chem. Int. Ed.* **2013**, *52*, 1420-1423; (g) Corey, E. J. *Angew. Chem. Int. Ed.* **2009**, *48*, 2100-2117; (h) Seguin, T. J.; Wheeler, S. E. *Angew. Chem. Int. Ed.* **2016**, *55*, 15889-15893; (i) Doney, A. C.; Rooks, B. J.; Lu, T.; Wheeler, S. E. *ACS Catal.* **2016**, *6*, 7948-7955; (j) Kennedy, C. R.; Guidera, J. A.; Jacobsen, E. N. *ACS Central Science* **2016**, *2*, 416-423; (k) Yamada, S.; Iwaoka, A.; Fujita, Y.; Tsuzuki, S. *Org. Lett.* **2013**, *15*, 5994-5997; (l) Lyngvi, E.; Bode, J. W.; Schoenebeck, F. *Chem. Sci.* **2012**, *3*, 2346-2350; (m) Samanta, R. C.; De Sarkar, S.; Frohlich, R.; Grimme, S.; Studer, A. *Chem. Sci.* **2013**, *4*, 2177-2184; (n) Lau, V. M.; Gorin, C. F.; Kanan, M. W. *Chem. Sci.* **2014**, *5*, 4975-4979; (o) Lau, V. M.; Pfalzgraff, W. C.; Markland, T. E.; Kanan, M. W. *J. Am. Chem. Soc.* **2017**, *139*, 4035-4041.

Insert Table of Contents artwork here